Title

Intrinsic connectivity network disruption in progressive supranuclear palsy

Journal

Annals of Neurology, 73(5)

ISSN

0364-5134

Authors

Gardner, Raquel C

Boxer, Adam L

Trujillo, Andrew

et al.

Publication Date

2013-05-01

DOI

10.1002/ana.23844

Peer reviewed

Published in final edited form as:
Ann Neurol. 2013 May ; 73(5): 603–616. doi:10.1002/ana.23844.

Intrinsic connectivity network disruption in progressive supranuclear palsy

Raquel C. Gardner, M.D.*, **Adam L. Boxer, M.D., Ph.D.***, **Andrew Trujillo, B.A.***, **Jacob B. Mirsky, M.A.**, **Christine C. Guo, Ph.D.**, **Efstathios D. Gennatas, M.B.B.S.**, **Hilary W. Heuer, Ph.D.**, **Eric Fine, Ph.D.**, **Juan Zhou, Ph.D.**, **Joel H. Kramer, Psy.D.**, **Bruce L. Miller, M.D.**, and **William W. Seeley, M.D.**
Memory and Aging Center, Department of Neurology, University of California, San Francisco

Abstract

Objective—Progressive supranuclear palsy (PSP) has been conceptualized as a large-scale network disruption, but the specific network targeted has not been fully characterized. We sought to delineate the affected network in patients with clinical PSP.

Methods—Using task-free fMRI, we mapped intrinsic connectivity to the dorsal midbrain tegmentum (dMT), a region which shows focal atrophy in PSP. Two healthy control groups (1 young, 1 older) were used to define and replicate the normal connectivity pattern, and patients with PSP were compared to an independent matched healthy control group on measures of network connectivity.

Results—Healthy young and older subjects showed a convergent pattern of connectivity to the dMT, including brainstem, cerebellar, diencephalic, basal ganglia, and cortical regions involved in skeletal, oculomotor, and executive control. Patients with PSP showed significant connectivity disruptions within this network, particularly within cortico-subcortical and cortico-brainstem interactions. Patients with more severe functional impairment showed lower mean dMT network connectivity scores.

Interpretation—This study defines a PSP-related intrinsic connectivity network in the healthy brain and demonstrates the sensitivity of network-based imaging methods to PSP-related physiological and clinical changes.

INTRODUCTION

Progressive supranuclear palsy syndrome (PSP-S) presents with progressive gait instability, axial rigidity, ophthalmoparesis, and cognitive-behavioral impairment.[1] Cognitive deficits often occur early and may include executive dysfunction, apraxia of speech, nonfluent aphasia, mental slowing, and cognitive inflexibility.[1–5] Behavioral symptoms, such as apathy, compulsions, obsessions, and utilization/imitation behavior, emerge at varied points along the course.[6] Typical PSP-S (also referred to as Richardson syndrome) features early, prominent gait and oculomotor symptoms that strongly predict underlying PSP pathology, a four-repeat tauopathy featuring characteristic neuronal and glial tau inclusions in basal ganglia, diencephalon, brainstem, cerebellum, and specific cortical regions.[7–9] In other patients with PSP pathology, cognitive or behavioral deficits arise first and may remain the most conspicuous feature.[9] Consistent with this clinical heterogeneity, PSP pathology is now classified as a subtype of frontotemporal lobar degeneration with tau-immunoreactive

Address correspondence to: William W. Seeley, MD, Box 1207, 675 Nelson Rising Lane, Suite 190, San Francisco, CA 94158, wseeley@memory.ucsf.edu.
*equal contributions

inclusions (FTLD-tau).[10] For clarity, throughout this manuscript we use PSP-S to refer to the typical PSP syndrome and PSP to refer to the histopathological entity.

PSP-S has long been proposed as a network-based disorder.[11–13] This concept rests on the observation that PSP-targeted regions feature robust axonal interconnections in non-human primates. The advent of "resting-state" or, perhaps preferably, "task-free" functional MRI (fMRI) has enabled researchers to identify large-scale intrinsic connectivity networks (ICNs) in humans by mapping regions with temporally correlated low frequency blood oxygen level-dependent signal fluctuations.[14] ICN mapping has been used to link healthy human network architectures to the cortically-predominant atrophy patterns seen in Alzheimer's disease and frontotemporal dementia.[15, 16] Early degeneration in typical PSP-S, however, targets subcortical and brainstem structures[17, 18] that have been less well characterized with ICN methods.[19] Because patients with PSP-S often lack severe cortical atrophy,[17, 18] cortical dysfunction in PSP-S has been proposed to reflect disconnection of cortical structures from their subcortical inputs and projection targets.[20, 21]

We hypothesized that ICN analysis would identify a PSP-related network in healthy subjects and that patients with PSP-S would show connectivity breakdowns within this ICN, even when volumetric changes are incorporated into the analysis. We further sought to explore relationships between connectivity disruption and clinical impairment. Our findings identify a dorsal midbrain-anchored, PSP-related anatomical system in humans and illustrate the sensitivity of ICN methods to network dysfunction and clinical severity in patients with PSP-S.

SUBJECTS AND METHODS

Subjects

Controls—Functional and structural MRI scans from 25 young healthy controls (HC1) were acquired from the New York University (NYU) test-retest dataset (10 males/15 females; ages 22–49; http://www.nitrc.org/frs/?group_id=274) generously made available by Milham and colleagues. As described in the primary publication,[22] these subjects had no history of psychiatric or neurological illness. For our ICN analyses, we used the first scans provided for each NYU subject. To validate our HC1 ICN findings and extend the analysis to healthy older controls, a second healthy control group (HC2) was selected from the UCSF Memory and Aging Center database. HC2 consisted of 26 right-handed subjects (13 females) between 60 and 70 years of age. Finally, a third healthy control group (HC3; N = 36, 24 females, see Table) was selected for comparison to the PSP-S group. HC3 was composed of two healthy control subjects matched to each patient with PSP-S for age, gender, handedness, and education. HC2 and HC3 subjects did not overlap; they were recruited from the San Francisco community through advertisements and underwent a neurological examination and neuropsychiatric assessments as described previously.[23] All were required to have a Clinical Dementia Rating (CDR) scale total score of 0, a Mini-Mental State Examination (MMSE) score of 27 or higher, no significant history of neurological disease or structural lesion on MRI, and a consensus diagnosis of cognitively normal. Diagnoses were rendered within 180 days of MRI scanning in all but two subjects, who were diagnosed as cognitively normal within a year prior to and after scanning. Quantitative eye movement evaluation was performed in 24 of the HC3 subjects within 90 days of scanning using methods described previously.[24]

Patients—The PSP-S group consisted of 18 patients with a diagnosis of "probable PSP" based on published consensus clinical diagnostic criteria.[25] This group included all patients in the UCSF database who (1) received a research diagnosis of probable PSP within 180 days of MRI, (2) had undergone task-free fMRI, (3) had no significant history of other

neurological disease or structural pathology on MRI (aside from changes consistent with PSP-S), and (4) had measured head movement < 3 mm translation and 3 degrees rotation. Twenty patients met criteria 1–3; two were excluded due to excessive movement. Sixteen of 18 patients with PSP-S were taking central nervous system acting medications at the time of the neuroimaging and clinical evaluations, including 9 patients who were taking dopaminergic medications (see Supplementary Methods for details). Patients underwent a thorough clinical evaluation including a history, general neurological examination, MMSE, and Clinical Dementia Rating Scale (CDR) by a staff behavioral neurologist within 90 days of scanning. Most patients were further evaluated with a bedside neuropsychological screen (n=12), the PSP rating scale[26] (PSPRS, n=14), the Unified Parkinson's Disease Rating Scale (UPDRS, n=14), and quantitative eye movement evaluation[24] (n=13) all within 90 days of scanning. A subset of the patients with PSP-S was recruited as part of a pilot clinical treatment trial; all patients, however, underwent MRI before study drug administration. Four of eighteen patients studied had died by the time of this writing, and all four underwent autopsy. Of these, all 4 had a primary neuropathological diagnosis of PSP.

All subjects or their surrogates provided informed consent prior to participation, and all study procedures were approved by the local institutional review boards.

Image acquisition

NYU dataset—MR imaging of NYU young healthy controls (HC1) was obtained on a Siemens Allegra 3.0 Tesla scanner. A T1-weighted magnetization prepared gradient echo (MP-RAGE) sequence was also obtained [time to repetition (TR) 2500 ms, time to echo (TE) 4.35 ms, time to inversion (TI) 900ms, flip angle 8 degrees, 176 slices, field of view 256 mm]. Task-free fMRI scans were obtained over 6.5 minutes, during which subjects were instructed to relax with eyes open, using a T2*-weighted sequence [TR 2000 ms, TE 25 ms, flip angle 90 degrees, 39 slices, matrix size 64 × 64, field of view 192 mm, acquisition voxel size 3 × 3 × 3 mm, 197 volumes].

UCSF dataset—MR imaging of older controls (HC2 and HC3) and patients with PSP occurred at the UCSF Neuroscience Imaging Center (NIC) on a Siemens Trio 3.0 Tesla scanner. For coregistration purposes, a volumetric magnetization prepared rapid gradient echo (MPRAGE) MRI sequence was used to obtain a T1-weighted image of the entire brain in sagittal slices during the same session (TR: 2300 ms; TE: 2.98 ms; inversion time, 900 ms; FA, 9°). These images were reconstructed as a 160 × 240 × 256 matrix with 1 mm^3 spatial resolution. Task-free fMRI images were obtained using an eight minute T2*-weighted sequence, during which subjects were instructed to remain awake with their eyes closed. Thirty-six interleaved axial slices (3 mm thick including a gap of 0.6 mm) were imaged parallel to the plane connecting the anterior and posterior commissures using a T2*-weighted echo planar imaging sequence [TR: 2000 ms; TE: 27 ms; flip angle: 80°; field of view: 230 × 230 mm^2; matrix size: 92 × 92; in-plane voxel size: 2.5 × 2.5 mm] with an online gradient adjustment for head motion compensation.

Image preprocessing and analysis

Structural Imaging—Using the SPM8 VBM8 toolbox, the PSP-S and HC3 T1-weighted images were processed using the VBM8 default estimation settings, segmented into grey and white matter, spatially normalized with the SPM8 default low-dimensional spatial normalization, subjected to a light cleanup (to remove any remaining non-brain tissue from the data), modulated, corrected for non-linear warping only, and smoothed with a 12 mm full width at half maximum isotropic Gaussian kernel. Correction for total intracranial volume was not performed as non-linear modulation and normalization corrects for variations in brain size. The resulting grey and white matter maps were subsequently used to

assess the atrophy pattern in our PSP-S group, model the effects of brain structure on intrinsic connectivity in PSP-S, and compare the utility of ICN and VBM approaches for detecting PSP-S-related changes.

Functional imaging: head motion assessment—Subject head motion was assessed by using the rigid body parameters provided by the realign algorithm in SPM5. Parameters for a given volume in the timeseries were compared to the parameters for the previous volume, creating a set of values that captured the amplitude of volume-to-volume changes. Using these values, mean root-mean-square (RMS) values were calculated for translation and mean Euler angles for rotation, as these summary metrics have been shown to correlate with network connectivity strength.[27] The PSP-S and HC3 groups showed no significant differences in translational or rotational movement (see Table).

Functional imaging: preprocessing and ROI-based intrinsic connectivity analysis—Using SPM5, UCSF subjects' functional images were spatially realigned, slice time corrected, coregistered to each subject's structural T1-weighted image, normalized to the Montreal Neurological Institute (MNI) T1 template, and smoothed with a 4 mm Gaussian kernel. Handling of NYU images was identical except that the functional images were normalized directly to the SPM5 EPI template.

Consistent with our previous approaches,[15] we selected a seed for the ROI-based ICN analysis from regions shown to be significantly atrophied in a previous VBM study performed at our center on an independent (non-overlapping) group of patients with PSP-S.[17] Among the six grey matter regions previously identified, we selected the dorsal midbrain tegmentum (dMT) because, in contrast to the other regions, the dMT was seated further from the subarachnoid space (mitigating concerns regarding mixed tissue compartment signals) and fell within a region imaged in all subjects (unlike the pontine tegmentum region, which fell partly outside the inferior edge of the task-free fMRI bounding box for some subjects). Further supporting this seed choice, recent clinico-anatomical studies have shown that dMT volume correlates with vertical saccade velocity, a function classically impaired in typical PSP-S.[28] The dMT ROI consisted of a 4 mm radius sphere centered at the local maximum from the previous VBM study comparing PSP-S to controls (5, −15, −8).[17] Using SPM8, we calculated the average BOLD signal intensity of all voxels within this ROI at each TR over each subject's eight-minute scan. We used the resulting time series as a covariate of interest in a whole-brain statistical parametric regression analysis to derive images corresponding to the dMT intrinsic functional correlation map for each subject. A total of six 4 mm radius spherical ROIs embedded in the CSF (left posterior and right anterior lateral ventricles) and white matter (left and right frontal and left and right parietal corona radiata) were included as covariates to reduce effects of physiological noise. We omitted the global signal and motion parameters as nuisance covariates based on recent work showing that inclusion of these measures exerts a negative effect (global signal regression) or no effect (motion parameters) on ICN test-retest reliability[29] and may unnecessarily reduce fMRI signal (motion parameters).[30] One sample t-tests were performed separately in HC1 and HC2 to identify clusters with significant intrinsic connectivity to the dMT in healthy young and older subjects at a cluster-forming height threshold of $p < 0.0001$ uncorrected and a cluster extent threshold of $p < 0.001$ corrected for family-wise error. To identify smaller brainstem and subcortical regions with highly significant correlation to the dMT, we also visualized the HC1, HC2, and HC1/HC2 overlap maps at a voxel-level, family-wise error-corrected threshold of $p < 0.05$ (no extent threshold). We employed this rigorous discovery (HC1) and replication (HC2) strategy because few previous ROI-based ICN studies have focused on brainstem ROIs and to ensure that the novel ICN delineated here showed topographical consistency across the adult age spectrum, consistent with other more extensively studied ICNs.[31, 32]

To compare the strength of the dMT-associated ICN in PSP-S to healthy matched controls (HC3), we entered the PSP-S and HC3 subject-level ICN maps into a second-level, random effects analysis masked to voxels for which non-zero fMRI signal was present in all subjects (to avoid including brainstem regions covered in some but not all subjects). Two-sample t-tests were performed to evaluate linear contrasts representing PSP-S < HC3 and PSP-S > HC3. Next, we used the BPM toolbox[33] to enter each subject's VBM grey and white matter maps as voxel-wise covariates to control for the effects of atrophy on ICN strength. Results of atrophy-uncorrected and corrected two-sample t-tests were thresholded using joint probability distribution thresholding[34] with joint height and extent thresholds of $p < 0.01$ and $p < 0.05$ (for visualization purposes), corrected across the search volume, in keeping with our previous work.[35] For these analyses, we applied an explicit dMT-seeded ICN mask, derived from the HC2 group one-sample t-test (voxel height threshold of $p < 0.005$ uncorrected, extent threshold of $p < 0.01$), chosen to generously constrain the search volume to regions within the dMT-associated ICN.

Functional imaging: ICN node pair matrix-based analysis and graph theoretical metrics—Because the seed ROI-based method only provides information about each voxel's connectivity to the chosen seed ROI, we used the HC2-derived dMT-seeded ICN, to create a group of "intrinsic connectivity clusters" for an ROI matrix-based analysis, allowing us to examine all pairwise ROI interactions. Cluster ROI creation followed methods described in the Supplementary Materials. The mean voxel-wise BOLD signal timeseries for each resulting ROI was used to create partial correlation matrices, with all other ROIs, that represent the ROI pair-wise correlation coefficients after controlling for white matter and CSF nuisance regressors. These group-level pair-wise correlations were visualized as matrices to facilitate assessment of connectivity reduction patterns in PSP-S. Two-sample t-tests identified ROI pair-wise differences in intrinsic connectivity between the PSP and HC3 groups, thresholded using false discovery rate correction for multiple comparisons at $p < 0.05$.

To augment the matrix-based ICN analyses described above, we used the methods of graph theory[36] to further characterize the normal network architecture and to derive metrics for group-level contrasts. In graph theoretical terms, each ROI represents a node, and the connectivity between each pair of ROIs represents an edge. We used the ICN matrices from the HC2 group to generate a graph in Cytoscape (http://www.cytoscape.org) based on an edge-weighted, force-directed layout algorithm that configures the nodes in space according to the weights of their edges, in this case based on the node pair correlation coefficients transformed to z-scores and thresholded at $z > 0.31$ ($r = 0.3$). To gauge the sensitivity of network architecture to matrix thresholding, we generated two further graphs, one with a more lenient and another with a more stringent threshold (Supplementary Figure 3).

To further explore differences between PSP and HC3 with regard to network architecture, we calculated total flow, mean clustering coefficient, and mean path length from the adjacency matrices for each subject, thresholded using the same three thresholds used to generate the HC2 graphs. Total flow is a measure of weighted degree, computed as the sum of a node's weighted pairwise connections. Clustering coefficient is a node-wise metric that captures the degree to which a node's 1st level neighbors are connected to one another. Path length describes to the shortest connectional distance required to travel between two given nodes in the graph. Two-sample t-tests were used to compare nodal total flow and clustering coefficient values between PSP-S and HC3, thresholded using false discovery rate correction for multiple comparisons at $p < 0.05$. Mean total flow, clustering coefficient, and path length were compared between groups using Mann-Whitney U tests performed for each HC2 graph threshold. Equations used to calculate graph metrics were implemented in

Matlab using the Brain Connectivity Toolbox and MatlabBGL (http://www.cs.purdue.edu/homes/dgleich/packages/matlab_bgl/).[37]

Correlation between dMT-associated ICN connectivity and clinical severity— To assess the relationship between PSP-S clinical severity and intrinsic connectivity, we derived a dMT-asociated ICN score for each patient with PSP-S. This score was computed as the mean beta value across all voxels of each subject's dMT-associated ICN map within an HC2-derived dMT network mask (thresholded at a joint height and extent threshold of $p < 0.001$). Because the resulting ICN scores were non-normally distributed within the PSP-S group, we used Spearman correlation to examine the relationship between mean dMT ICN score and CDR sum of boxes, UPDRS, and PSPRS. These clinical measures were chosen because they summarize clinical severity in PSP and showed ample dynamic range without floor or ceiling effects. In addition, we examined Spearman correlations between mean dMT ICN score and vertical saccade velocity, measured in degrees per second. Age, gender, and movement parameters showed no significant correlation with the dMT-associated ICN score, and these potential confounders were therefore omitted from the analyses to improve power.

Comparisons between ICN and VBM findings in PSP-S—In an exploratory analysis, we compared the sensitivity of task-free fMRI and VBM analyses for detecting network degeneration in PSP-S. At each voxel, effect size for the PSP < HC3 contrast was calculated using voxel-wise group means and pooled standard deviations derived from the subject-level ICN or VBM grey matter maps. Maps were created to visualize where ICN analysis generated a greater effect size than VBM and vice versa (see Supplementary Methods).

Statistical thresholding principles for image analyses—A consistent thresholding strategy was used for the primary imaging analyses. One-sample t-tests for network definition were thresholded at a cluster-forming height threshold of $p < 0.0001$ and a cluster extent threshold of $p < 0.001$ corrected for family-wise error across the whole brain. Major study hypotheses (2 sample t-tests comparing PSP-S to HC3) were tested at a joint height and extent threshold of $p < 0.01$ as well as $p < 0.05$ (for visualization purposes), cluster-level corrected across the search volume.[34] Thresholds not used for hypothesis testing were guided by their specific purpose. For example, network masks were thresholded to generously constrain group-level analyses to a specific ICN without expanding the search volume to the entire brain.

RESULTS

The healthy brain features an ICN composed of PSP-vulnerable brain regions

Our first goal was to identify a healthy brain network composed of regions known to degenerate in PSP-S. To pursue this objective, we conducted ICN analyses in two independent healthy control groups (young (HC1) and older (HC2) controls). Using ROI-based task-free fMRI analysis, we identified regions that showed significant intrinsic connectivity with the dMT, a primary focus of grey matter atrophy in PSP-S[17] that correlates with vertical saccade velocity in patients with PSP-S and other neurodegenerative disorders.[28] As expected, the ICNs converged in the healthy young and older control "network discovery and replication" groups (HC1 and HC2; Figure 1). Despite seeding this ICN analysis with a focal midbrain ROI, we detected a distributed network pattern that included additional brainstem, cerebellar, diencephalic, basal ganglia, and cortical regions known to degenerate along differing gradients in typical and atypical PSP-S.[9] and to cooperate in the healthy brain to support skeletal and ocular motor function, gait, action

planning, and cognitive-behavioral control. Because prominent behavioral and speech praxis deficits can accompany typical PSP-S, we noted with interest that the dMT-associated ICN also included the pregenual anterior cingulate and frontoinsular cortices, which show early degeneration in the behavioral variant of frontotemporal dementia (bvFTD),[38] as well as the frontal operculum/dorsal anterior insula, a focus of atrophy in patients with nonfluent aphasia and apraxia of speech.[39] Importantly, the dMT-associated ICN was consistent across different adult age groups, scanners, and acquisition protocols, confirming that it represents a robust and reproducible ICN.

PSP-S is associated with reduced connectivity throughout the dorsal midbrain tegmentum-associated ICN

Next, we sought network connectivity changes in patients with PSP-S. Compared to 36 matched healthy controls (HC3), patients with PSP-S showed distributed network connectivity reductions throughout the dMT-seeded ICN (Figure 2, Supplementary Table 1), most prominent in striatum, thalamus, cerebellum, and cortical regions. Omitting the dMT-associated network mask revealed minimal changes; a few clusters of reduced connectivity in PSP-S extended just beyond the mask boundaries or into contiguous regions, such as the superior and middle temporal gyri. Importantly, no regions of increased connectivity were identified in PSP-S vs. controls (with or without masking) even at the lower statistical threshold included in Figure 2 for visualization purposes. After atrophy correction, the PSP-S < HC3 contrast differed little, with only the dorsal midbrain and SMA showing less extensive dMT connectivity reduction in PSP-S (Supplementary Figure 2). No regions of increased connectivity in PSP-S were identified in the atrophy-corrected model.

PSP-S is associated with distributed node pair connectivity reductions throughout the dorsal midbrain tegmentum-associated ICN matrix

To map a more comprehensive network architecture among the regions identified with the seed ROI-based approach, we created data-driven ROIs representing the major nodes of the dMT-associated ICN (Figure 3, Supplementary Figure 1, Supplementary Table 2, clusters available upon request from the corresponding author). PSP-S showed pair-wise connectivity reductions distributed throughout this matrix (Figure 3E), especially in cortico-subcortical and cortico-brainstem connections. No node pair connection showed increased connectivity. This analysis extended the seed-based ICN findings by showing that regions distributed throughout this neural system show reduced connectivity with each other, not only with the dMT.

The healthy configuration of the fully specified network is graphed in Figure 4 using an edge-weighted, force-directed algorithm to capture nodes' relationships with each other. This approach illustrated the centrality of the mesothalamic junction (MTJ, just rostral to the dMT), basal ganglia (a cluster spanning anterior caudate, putamen, and pallidum), and thalamus. These "hub-like" nodes feature high degree centrality and provide a functional link between the cortex and brainstem/cerebellum. Comparing each node's total flow (the sum of its weighted edges) in PSP-S and HC3, we identified the MTJ and several key cortical regions as showing significant total flow reductions in PSP-S (Figure 4). All network nodes showed reduced clustering coefficients in PSP-S (FDR-corrected, $p < 0.05$). Mean total flow and clustering coefficient (computed across all nodes) showed significant reductions in PSP-S (Supplementary Table 3). No significant differences were found for mean path length at any of the three HC2 graph thresholds.

PSP-S connectivity reductions correlate with clinical impairment

To explore whether ICN measures prove sensitive to disease severity, we assessed correlations between the mean dMT-associated ICN score (see Methods) and clinical

measures that summarize functional integrity. Initially, no significant correlations were found. Examination of these data, however, revealed one conspicuous outlier: a patient with PSP-S having severe clinical impairment despite a relatively high mean dMT-associated ICN score. Excluding this outlier recovered a significant inverse relationship between mean dMT-associated ICN strength and the CDR sum of boxes score ($\rho = -0.662$, $p = 0.004$; Figure 5), indicating that patients with more advanced disease showed weaker network connectivity. Similar but non-significant negative correlations were seen for the PSPRS ($\rho = -0.345$, $p = 0.249$) and UPDRS ($\rho = -0.319$, $p = 0.288$) with the outlier excluded. We further observed a trend toward slower downward saccades in patients with lower ICN scores ($\rho = 0.511$, $p = 0.074$; outlier included). Importantly, patients with PSP-S who were or were not taking dopaminergic agents showed no difference in mean dMT connectivity ($t = 0.409$, $p = 0.688$), a finding which held after exclusion of the outlier in the connectivity-behavior correlation analyses, who was taking carbidopa/levodopa ($t = 0.942$, $p = 0.361$).

Intrinsic connectivity and morphometric analyses play complementary roles in detecting network degeneration in PSP-S

Early detection and disease-monitoring PSP-S biomarkers may need to detect physiological changes that precede gross atrophy. We hypothesized that ICN analysis would prove more sensitive to early disease in regions with little or no atrophy while structural imaging (VBM), which involves less methodological noise, would outperform ICN methods in regions already showing significant atrophy. To test these ideas, we used the PSP-S < HC3 contrasts to compare the voxel-wise effect sizes of dMT connectivity reduction to those derived from VBM. As predicted, we found that dMT connectivity showed larger effect sizes in network regions functionally connected to areas where significant atrophy had already emerged. On the other hand, VBM generally produced larger effect sizes for regions already showing significant atrophy (Figure 6). These findings suggest that ICN and VBM approaches may provide complementary information and raise the speculation that ICN mapping may prove most valuable during early-stage disease.

DISCUSSION

This study establishes an ICN, anchored by the dorsal midbrain, whose nodes include the brainstem, basal ganglia, diencephalic, cerebellar, and cortical regions that show atrophy and tau aggregation in PSP.[1, 9, 17] Hence, PSP-S, like other neurodegenerative disease syndromes,[15] reflects injury to a specific large-scale cortical-subcortical system that can be mapped in the healthy brain with task-free fMRI. We further demonstrated that this method detects robust, distributed, and functionally relevant connectivity reductions in PSP-S within a network of skeletal and ocular motor control structures as well as in regions that participate in executive, social-emotional and speech-language functions. These findings suggest that the heterogeneous clinical presentations of PSP pathology may reflect the gradient of pathology within nodes of the broader network outlined here. Patients whose disease begins in the dorsal midbrain and its closest motor control system affiliates will present with typical PSP-S but would be predicted to later develop behavioral and language deficits when pathology reaches the relevant cortical network nodes. In contrast, patients whose pathology begins in cortical nodes may present with bvFTD, progressive nonfluent aphasia, or a corticobasal syndrome, depending on the node and hemisphere affected first, before disease spreads along network lines to produce the defining oculomotor and gait impairments that lead clinicians to predict PSP as the underlying histopathology. Perhaps most importantly, we found that intrinsic connectivity disruption correlated with overall clinical severity and detected PSP-S-related network dysfunction in regions lacking significant grey matter atrophy.

Relationship of present findings to PSP anatomical literature

Recently, Whitwell et al[40] performed a task-free fMRI analysis in patients with PSP-S. First, they performed a seed-based analysis using an ROI containing the entire bilateral thalami. Although several regions showed increased or decreased connectivity to this thalamic seed, it is difficult to place these results in an anatomical context given the diverse anatomical and intrinsic functional connections of the thalamus.[41] Second, these authors applied independent component analysis in healthy controls to identify a "basal ganglia network", which showed connectivity reductions in PSP-S compared to the same healthy controls. This strategy, using the same control subjects to select and analyze the network, reduces confidence in the reported group differences due to the problem of statistical dependency.[42] Here, we used a data-driven seed-based approach to define a reproducible dMT-associated network targeted in PSP-S compared to an independent sample of healthy controls. We observed no increases in network connectivity, perhaps reflecting the anatomical specificity of our approach.

The present work builds on a foundation of previous PSP-S neuropathological and imaging studies. Although the core pathological distribution of PSP has been recognized since the disorder's initial description,[1] more recent structural imaging and pathological analyses have shed light on the cortical vulnerability patterns associated with typical and atypical PSP.[9, 17, 18] Recent work using diffusion tensor imaging has underlined the role of white matter tract degeneration, especially within the superior cerebellar peduncle.[43, 44] Positron emission tomography studies analyzing the covariance of metabolic patterns across patients and controls have shown a PSP-related pattern that distinguishes PSP from other atypical parkinsonian syndromes[45] and includes many of the structures identified here with ICN fMRI.[46] Overall, these investigations converge on a core set of PSP-affected structures while suggesting that the anatomical pattern relates closely to the associated clinical syndrome. The present study advances this framework by delineating a specific dMT-associated large-scale network and demonstrating that task-free fMRI detects PSP-S-related connectivity breakdowns. Our results further outline a comprehensive architecture of node pair-wise connections for this system and show that PSP-S-related connectivity breakdowns emphasize cortico-subcortical and cortico-brainstem interactions and correlate with clinical severity. Although intrinsic brainstem circuits may also lose functional connectivity in PSP-S, connectivity between brainstem node pairs was less conspicuously affected in the present analyses. Whether this observation reflects PSP biology or methodological limitations requires further study.

Relationship of present findings to ICN literature on Idiopathic Parkinson's Disease (IPD)

Our PSP-S findings also fit into a context provided by a growing task-free fMRI literature on IPD. While some studies of patients with IPD off of dopaminergic agents have shown decreased connectivity between various cortical motor regions and basal ganglia,[47, 48] others have shown increased connectivity in sensorimotor circuits, specifically between dorsal caudal putamen, inferior temporal gyrus, anterior cingulate cortex, and superior frontal gyrus. These areas of increased connectivity diminished when the patients were rescanned on dopaminergic agents.[49] Fascinating recent work[50] suggested increased functional connectivity between the subthalamic nucleus and cortical motor areas in the off-medication state in IPD, supporting the notion of basal ganglia-thalamo-cortical circuit hypersynchronicity in IPD[51] and providing a possible mechanism for STN-targeted deep-brain stimulation. In contrast to the IPD findings, the matrix analysis performed here suggested decreased connectivity between thalamus, basal ganglia, and pre-SMA in PSP-S, even though half of the patients were not taking dopaminergic agents at the time of scanning. This contrast to IPD could reflect the severe STN tau pathology in PSP and explain, at least in part, why most patients with PSP-S do not respond to levodopa or STN

DBS treatment[52] and why we found no significant difference in mean dMT-associated network connectivity between patients on and off dopaminergic agents.

Insights revealed by matrix and graph theoretical analyses

Networks represent multiple nodal interactions between spatially distributed and functionally diverse regions. Seed-based ICN analysis can identify regions with abnormal connectivity to a chosen network node such as, in this case, the dMT. While this method works well for network identification, it provides no information about how network nodes interact with regions other than the seed. Including matrix and graph theoretical analyses enabled us to delineate the healthy dMT-associated network configuration and identify its hub-like nodes in the mesothalamic junction, basal ganglia, and thalamus. These nodes may serve as PSP-vulnerable network "epicenters" whose connectivity patterns predict degeneration severity throughout the network, as shown for other neurodegenerative disease syndromes.[53] Graph theoretical analyses revealed PSP-S-related reductions in nodal network traffic (total flow) and local interconnectivity (clustering coefficient). Additional work is needed to determine whether characterizing the heathy brain functional connectome can predict the pace and topography of progression in single patients with PSP-S and other neurodegenerative syndromes.

Clinical correlation

In PSP-S, a dMT-associated ICN summary score correlated with the CDR sum of boxes score, a measure of overall clinical severity. Similar but weaker correlations with the UPDRS, PSPRS, and downward saccade velocity may have escaped significance due to the smaller samples for which these data were available or because these measures sample too narrow a range of PSP-S-related deficits to correlate with average network connectivity. The outlier uncovered in these analyses had the fastest downward saccades within the PSP-S group, consistent with this patient's high dMT-ICN score. These observations raise important questions, including whether this patient has a non-PSP neuropathology, represents an atypical midbrain-sparing PSP presentation, or reflects method-related statistical noise. Despite these lingering questions, our cross-sectional findings suggest that ICN mapping merits further investigation as a potential disease-monitoring biomarker for longitudinal studies and treatment trials.

Sensitivity of intrinsic connectivity analysis to early-stage network degeneration

ICN analysis outperformed VBM in discriminating PSP-S from controls in network regions that lacked significant group-level atrophy. This finding hints at a potential role for ICN analysis in detecting early PSP-S-related changes. Longitudinal studies are needed to determine whether ICN data provide the "leading edge", sensitive to early network dysfunction and predicting where atrophy will emerge next. This capability would provide a much-needed index of early stage disease for patients genetically at-risk for PSP or other neurodegenerative diseases, especially once potential disease-modifying therapies enter clinical trials.

Limitations and Future Directions

This study focused on identifying a PSP-related ICN using novel network mapping methods. The analysis was not designed to provide a comprehensive multimodal neuroimaging comparison or to use imaging to predict pathology. Although the typical PSP syndrome we studied strongly predicts PSP pathology,[25] some patients in this study could have had a non-PSP histopathology, and future studies are needed to determine whether ICN measurements can single out patients with PSP-S who lack PSP pathology. Many patients studied here took medications to address ongoing motor or psychiatric/behavioral symptoms. These

medications could have influenced the ICN results, yet studying only medication-free patients with PSP-S would have proven unfeasible, even at our referral center where recruiting patients with PSP-S represents a major research priority. The noninvasive and repeatable nature of ICN methods make them attractive potential longitudinal biomarkers, and future work should explore this potential by studying patients with PSP and other network-based neurodegenerative disorders over time.

Supplementary Material

Refer to Web version on PubMed Central for supplementary material.

Acknowledgments

This work was supported by the Tau Consortium (grants to ALB, BLM, and WWS), the Larry L. Hillblom Foundation (grants to JHK and BLM), the Shupin Foundation (grant to RCG), and the NIH (NIA grants AG023501 to BLM and WWS, AG031278 and AG038791 to ALB, AG032289 to JHK, AG1657303 to BLM). We thank Dr. Michael Milham and colleagues, New York University School of Medicine, for providing public access to the young control fMRI dataset used here. Finally, we thank our patients and their families for their invaluable contributions to neurodegenerative disease research.

References

1. Steele JC, Richardson JC, Olszewski J. Progressive Supranuclear Palsy. Arch Neurol. 1964 Apr. 10:333–60. [PubMed: 14107684]
2. Josephs KA, Petersen RC, Knopman DS, et al. Clinicopathologic analysis of frontotemporal and corticobasal degenerations and PSP. Neurology. 2006 Jan 10; 66(1):41–8. [PubMed: 16401843]
3. Dubois B, Pillon B, Legault F, Agid Y, Lhermitte F. Slowing of cognitive processing in progressive supranuclear palsy. A comparison with Parkinson's disease. Arch Neurol. 1988 Nov; 45(11):1194–9. [PubMed: 3190499]
4. Pillon B, Blin J, Vidailhet M, et al. The neuropsychological pattern of corticobasal degeneration: comparison with progressive supranuclear palsy and Alzheimer's disease. Neurology. 1995; 45(8): 1477–83. [PubMed: 7644044]
5. Bak TH, Crawford LM, Hearn VC, Mathuranath PS, Hodges JR. Subcortical dementia revisited: similarities and differences in cognitive function between progressive supranuclear palsy (PSP), corticobasal degeneration (CBD) and multiple system atrophy (MSA). Neurocase. 2005; 11(4):268–73. [PubMed: 16093227]
6. Aarsland D, Litvan I, Larsen JP. Neuropsychiatric symptoms of patients with progressive supranuclear palsy and Parkinson's disease. Journal of Neuropsychiatry and Clinical Neurosciences. 2001 Winter;13(1):42–9. [PubMed: 11207328]
7. Schofield EC, Hodges JR, Macdonald V, Cordato NJ, Kril JJ, Halliday GM. Cortical atrophy differentiates Richardson's syndrome from the parkinsonian form of progressive supranuclear palsy. Mov Disord. 2010 Dec 13.
8. Hauw JJ, Daniel SE, Dickson D, et al. Preliminary NINDS neuropathologic criteria for Steele-Richardson-Olszewski syndrome (progressive supranuclear palsy). Neurology. 1994; 44(11):2015–9. [PubMed: 7969952]
9. Dickson DW, Ahmed Z, Algom AA, Tsuboi Y, Josephs KA. Neuropathology of variants of progressive supranuclear palsy. Curr Opin Neurol. 2010 Aug; 23(4):394–400. [PubMed: 20610990]
10. Mackenzie IR, Neumann M, Bigio EH, et al. Nomenclature and nosology for neuropathologic subtypes of frontotemporal lobar degeneration: an update. Acta Neuropathol. 2010 Jan; 119(1):1–4. [PubMed: 19924424]
11. Salmon E, Van der Linden MV, Franck G. Anterior cingulate and motor network metabolic impairment in progressive supranuclear palsy. NeuroImage. 1997; 5(3):173–8. [PubMed: 9345547]

12. Saper CB, Wainer BH, German DC. Axonal and transneuronal transport in the transmission of neurological disease: potential role in system degenerations, including Alzheimer's disease. Neuroscience. 1987; 23(2):389–98. [PubMed: 2449630]
13. Chen AL, Riley DE, King SA, et al. The disturbance of gaze in progressive supranuclear palsy: implications for pathogenesis. Front Neurol. 2010; 1:147. [PubMed: 21188269]
14. Fox MD, Raichle ME. Spontaneous fluctuations in brain activity observed with functional magnetic resonance imaging. Nat Rev Neurosci. 2007 Sep; 8(9):700–11. [PubMed: 17704812]
15. Seeley WW, Crawford RK, Zhou J, Miller BL, Greicius MD. Neurodegenerative diseases target large-scale human brain networks. Neuron. 2009; 62(1):42–52. [PubMed: 19376066]
16. Buckner RL, Snyder AZ, Shannon BJ, et al. Molecular, structural, and functional characterization of Alzheimer's disease: evidence for a relationship between default activity, amyloid, and memory. J Neurosci. 2005 Aug 24; 25(34):7709–17. [PubMed: 16120771]
17. Boxer AL, Geschwind MD, Belfor N, et al. Patterns of brain atrophy that differentiate corticobasal degeneration syndrome from progressive supranuclear palsy. Arch Neurol. 2006 Jan; 63(1):81–6. [PubMed: 16401739]
18. Josephs KA, Whitwell JL, Dickson DW, et al. Voxel-based morphometry in autopsy proven PSP and CBD. Neurobiol Aging. 2008 Feb; 29(2):280–9. [PubMed: 17097770]
19. Habas C, Kamdar N, Nguyen D, et al. Distinct cerebellar contributions to intrinsic connectivity networks. Journal of Neuroscience. 2009 Jul 1; 29(26):8586–94. [PubMed: 19571149]
20. Cummings JL, Benson DF. Subcortical dementia. Review of an emerging concept. Arch Neurol. 1984; 41:874–9. [PubMed: 6235797]
21. Foster NL, Gilman S, Berent S, Morin EM, Brown MB, Koeppe RA. Cerebral hypometabolism in progressive supranuclear palsy studied with positron emission tomography. Ann Neurol. 1988; 24(3):399–406. [PubMed: 3265862]
22. Shehzad Z, Kelly AM, Reiss PT, et al. The resting brain: unconstrained yet reliable. Cereb Cortex. 2009 Oct; 19(10):2209–29. [PubMed: 19221144]
23. Rosen HJ, Gorno-Tempini ML, Goldman WP, et al. Patterns of brain atrophy in frontotemporal dementia and semantic dementia. Neurology. 2002; 58(2):198–208. [PubMed: 11805245]
24. Boxer AL, Garbutt S, Seeley WW, et al. Saccade abnormalities in autopsy-confirmed frontotemporal lobar degeneration and Alzheimer disease. Archives of Neurology. 2012; 69(4): 509–17. [PubMed: 22491196]
25. Litvan I, Agid Y, Calne D, et al. Clinical research criteria for the diagnosis of progressive supranuclear palsy (Steele-Richardson-Olszewski syndrome): report of the NINDS-SPSP international workshop. Neurology. 1996; 47(1):1–9. [PubMed: 8710059]
26. Golbe LI, Ohman-Strickland PA. A clinical rating scale for progressive supranuclear palsy. Brain. 2007 Jun; 130(Pt 6):1552–65. [PubMed: 17405767]
27. Van Dijk KR, Sabuncu MR, Buckner RL. The influence of head motion on intrinsic functional connectivity MRI. NeuroImage. 2012; 59(1):431–8. [PubMed: 21810475]
28. Boxer AL, Garbutt S, Seeley WW, et al. Saccade abnormalities in autopsy-confirmed frontotemporal lobar degeneration and Alzheimer disease. Arch Neurol. Apr; 69(4):509–17. [PubMed: 22491196]
29. Guo CC, Kurth F, Zhou J, et al. One-year test-retest reliability of intrinsic connectivity network fMRI in older adults. NeuroImage. 2012; 61(4):1471–83. [PubMed: 22446491]
30. Churchill NW, Oder A, Abdi H, et al. Optimizing preprocessing and analysis pipelines for single-subject fMRI. I. Standard temporal motion and physiological noise correction methods. Hum Brain Mapp. Mar; 33(3):609–27. [PubMed: 21455942]
31. Biswal BB, Mennes M, Zuo XN, et al. Toward discovery science of human brain function. Proc Natl Acad Sci U S A. Mar 9; 107(10):4734–9. [PubMed: 20176931]
32. Allen EA, Erhardt EB, Damaraju E, et al. A baseline for the multivariate comparison of resting-state networks. Front Syst Neurosci. 5:2. [PubMed: 21442040]
33. Casanova R, Srikanth R, Baer A, et al. Biological parametric mapping: A statistical toolbox for multimodality brain image analysis. NeuroImage. 2007; 34(1):137–43. [PubMed: 17070709]

34. Poline JB, Worsley KJ, Evans AC, Friston KJ. Combining spatial extent and peak intensity to test for activations in functional imaging. NeuroImage. 1997; 5(2):83–96. [PubMed: 9345540]
35. Zhou J, Greicius MD, Gennatas ED, et al. Divergent network connectivity changes in behavioural variant frontotemporal dementia and Alzheimer's disease. Brain. 2010 May; 133(Pt 5):1352–67. [PubMed: 20410145]
36. Bullmore E, Sporns O. Complex brain networks: graph theoretical analysis of structural and functional systems. Nat Rev Neurosci. 2009 Mar; 10(3):186–98. [PubMed: 19190637]
37. Rubinov M, Sporns O. Complex network measures of brain connectivity: uses and interpretations. Neuroimage. 2010 Sep; 52(3):1059–69. [PubMed: 19819337]
38. Seeley WW, Crawford R, Rascovsky K, et al. Frontal paralimbic network atrophy in very mild behavioral variant frontotemporal dementia. Arch Neurol. 2008 Feb; 65(2):249–55. [PubMed: 18268196]
39. Nestor PJ, Graham NL, Fryer TD, Williams GB, Patterson K, Hodges JR. Progressive non-fluent aphasia is associated with hypometabolism centred on the left anterior insula. Brain. 2003 Nov; 126(Pt 11):2406–18. [PubMed: 12902311]
40. Whitwell JL, Avula R, Master A, et al. Disrupted thalamocortical connectivity in PSP: a resting-state fMRI, DTI, and VBM study. Parkinsonism Relat Disord. Sep; 17(8):599–605. [PubMed: 21665514]
41. Kim DJ, Park B, Park HJ. Functional connectivity-based identification of subdivisions of the basal ganglia and thalamus using multilevel independent component analysis of resting state fMRI. Hum Brain Mapp. Feb 14.
42. Kriegeskorte N, Simmons WK, Bellgowan PS, Baker CI. Circular analysis in systems neuroscience: the dangers of double dipping. Nat Neurosci. 2009 May; 12(5):535–40. [PubMed: 19396166]
43. Canu E, Agosta F, Baglio F, Galantucci S, Nemni R, Filippi M. Diffusion tensor magnetic resonance imaging tractography in progressive supranuclear palsy. Mov Disord. 2011 Apr 15.
44. Whitwell JL, Master AV, Avula R, et al. Clinical correlates of white matter tract degeneration in progressive supranuclear palsy. Arch Neurol. 2011 Jun; 68(6):753–60. [PubMed: 21670399]
45. Tang CC, Poston KL, Eckert T, et al. Differential diagnosis of parkinsonism: a metabolic imaging study using pattern analysis. Lancet Neurol. 2010 Feb; 9(2):149–58. [PubMed: 20061183]
46. Eckert T, Tang C, Ma Y, et al. Abnormal metabolic networks in atypical parkinsonism. Mov Disord. 2008 Apr 15; 23(5):727–33. [PubMed: 18186116]
47. Wu T, Long X, Wang L, et al. Functional connectivity of cortical motor areas in the resting state in Parkinson's disease. Hum Brain Mapp. Sep; 32(9):1443–57. [PubMed: 20740649]
48. Helmich RC, Derikx LC, Bakker M, Scheeringa R, Bloem BR, Toni I. Spatial remapping of cortico-striatal connectivity in Parkinson's disease. Cereb Cortex. May; 20(5):1175–86. [PubMed: 19710357]
49. Kwak Y, Peltier S, Bohnen NI, Muller ML, Dayalu P, Seidler RD. Altered resting state cortico-striatal connectivity in mild to moderate stage Parkinson's disease. Front Syst Neurosci. 4:143. [PubMed: 21206528]
50. Baudrexel S, Witte T, Seifried C, et al. Resting state fMRI reveals increased subthalamic nucleus-motor cortex connectivity in Parkinson's disease. Neuroimage. Apr 15; 55(4):1728–38. [PubMed: 21255661]
51. Hammond C, Bergman H, Brown P. Pathological synchronization in Parkinson's disease: networks, models and treatments. Trends Neurosci. 2007 Jul; 30(7):357–64. [PubMed: 17532060]
52. van Balken I, Litvan I. Current and future therapeutic approaches in progressive supranuclear palsy. Handb Clin Neurol. 2008; 89:493–508. [PubMed: 18631772]
53. Zhou J, Gennatas ED, Kramer JH, Miller BL, Seeley WW. Predicting regional neurodegeneration from the healthy brain functional connectome. Neuron. 2012; 73(6):1216–27. [PubMed: 22445348]

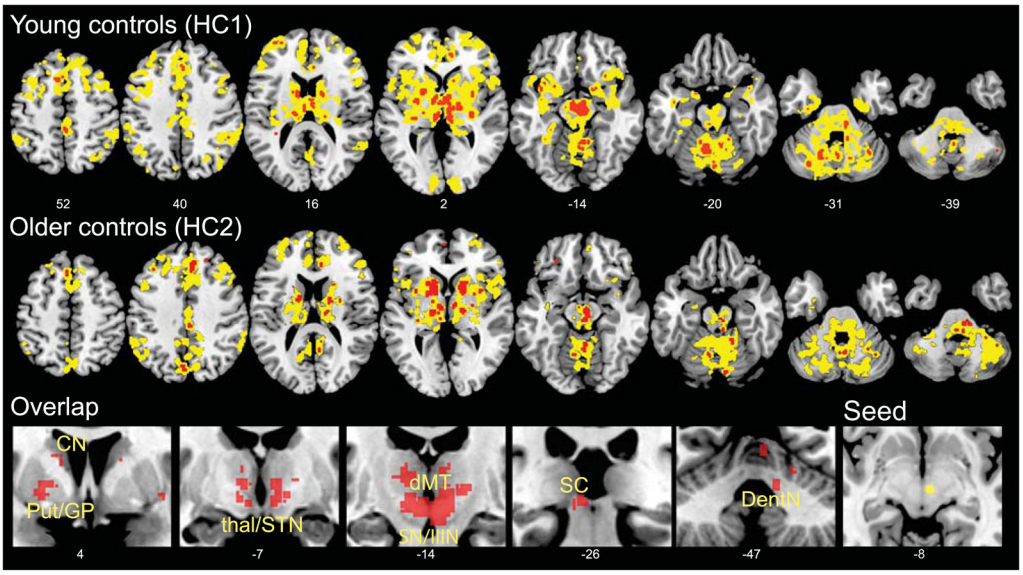

Figure 1. The dMT-associated ICN

The dMT was used as a seed ROI for voxel-wise task-free fMRI analyses in healthy young (HC1, upper row) and older (HC2, middle row) controls. Results are displayed at height threshold $p < 0.0001$, extent threshold $p < 0.001$ family-wise error-corrected at the cluster level (yellow) and at height threshold $p < 0.05$, family-wise error-corrected at the voxel level (red) to avoid omitting small but significant brainstem clusters. Corrections were performed across the whole brain. The overlap between the voxel level results for the two control groups (bottom row) is shown to highlight the consistency of the pattern within subcortical, diencephalic, and brainstem/cerebellar structures central to the known PSP pathological injury pattern. The right-most panel in the bottom row shows an axial view of the dMT seed (yellow) used for the seed-based ICN analysis. Slice labels reflect MNI coordinates. The right side of the images corresponds to the right side of the brain. CN, caudate nucleus; dMT, dorsal midbrain tegmentum; DentN, dentate nucleus; GPe, globus pallidus externa; latCRB, lateral cerebellum; Put, putamen; SC, superior colliculus; SN, substantia nigra; STN, subthalamic nucleus; IIIN, third nerve nuclear complex.

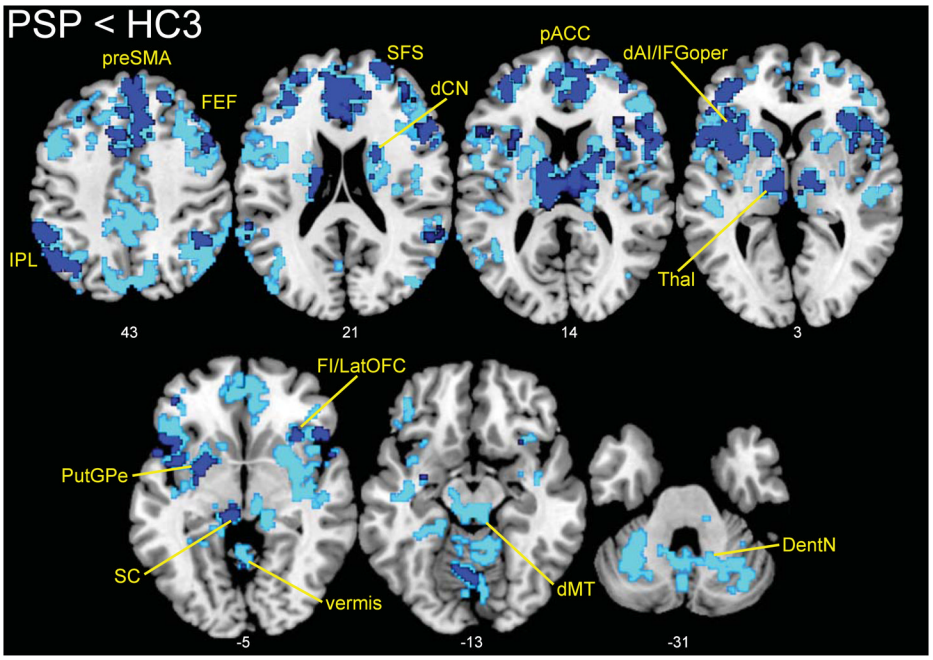

Figure 2. Network connectivity reductions in PSP

Examining the same dMT-associated ICN shown in Figure 1, we found connectivity reductions in PSP distributed throughout the network. Results are displayed at $p < 0.01$ (dark blue) and $p < 0.05$ (light blue), joint height and extent corrected at the cluster level across the network. Slice labels reflect MNI coordinates. The right side of the images corresponds to the right side of the brain. dAI, dorsal anterior insula; dCN, dorsal caudate nucleus; FEF, frontal eye fields; FI, frontoinsula; IFGoper, inferior frontal gyrus (pars opercularis); IPL, inferior parietal lobule; latOFC, lateral orbitofrontal cortex; Thal, thalamus; pACC, pregenual ACC; preSMA, pre-supplementary motor area; SFS, superior frontal sulcus. Other abbreviations as in Figure 1.

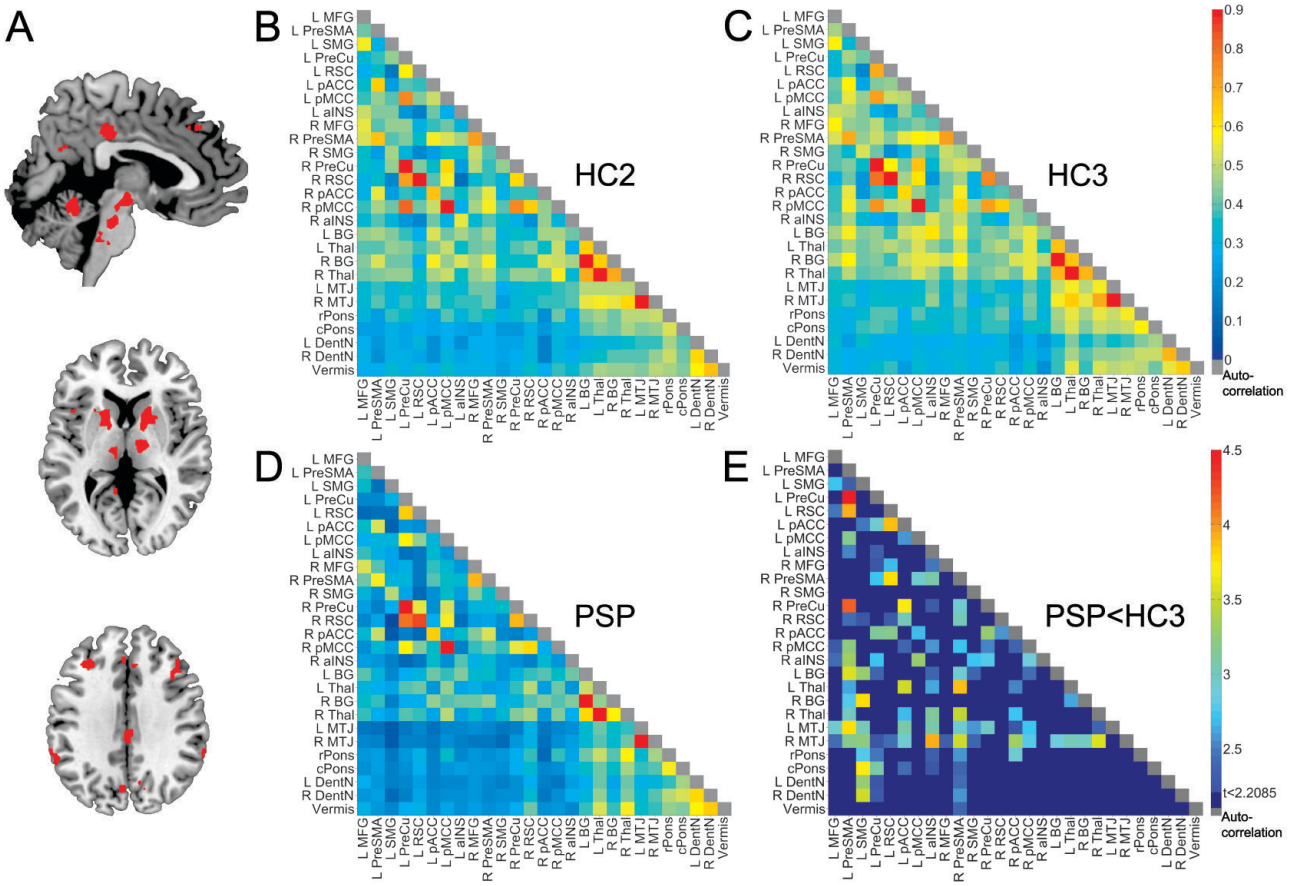

Figure 3. The broader PSP-related network in health and disease

Regions showing intrinsic connectivity to the dMT in the HC2 group were isolated (**A**, Supplementary Figure 1, Supplementary Table 2) and used to generate matrices representing the connectivity strength between each ROI pair for HC2 (**B**), HC3 (**C**), and PSP (**D**). Color bars in **B–D** indicate the Pearson correlation coefficients (r) derived for each node pair transformed to z-scores. In (**E**), the node pair matrix highlights those pairs showing significant connectivity reduction in PSP vs. HC3, corrected at the matrix level for false discovery rate to produce a $p < 0.05$ ($z \geq 2.21$). The color bar indicates the z-scores derived from the two-sample t-test (PSP < HC3). Colored node pairs indicate significant reductions. aINS, anterior insula; BG, basal ganglia; cPONS, caudal pons; MFG, middle frontal gyrus; MTJ, mesothalamic junction; pMCC, posterior midcingulate cortex; PreCu, precuneus; rPONS, rostral pons; RSC, retrosplenial cortex; SMG, supramarginal gyrus. Other abbreviations as in Figures 1 & 2.

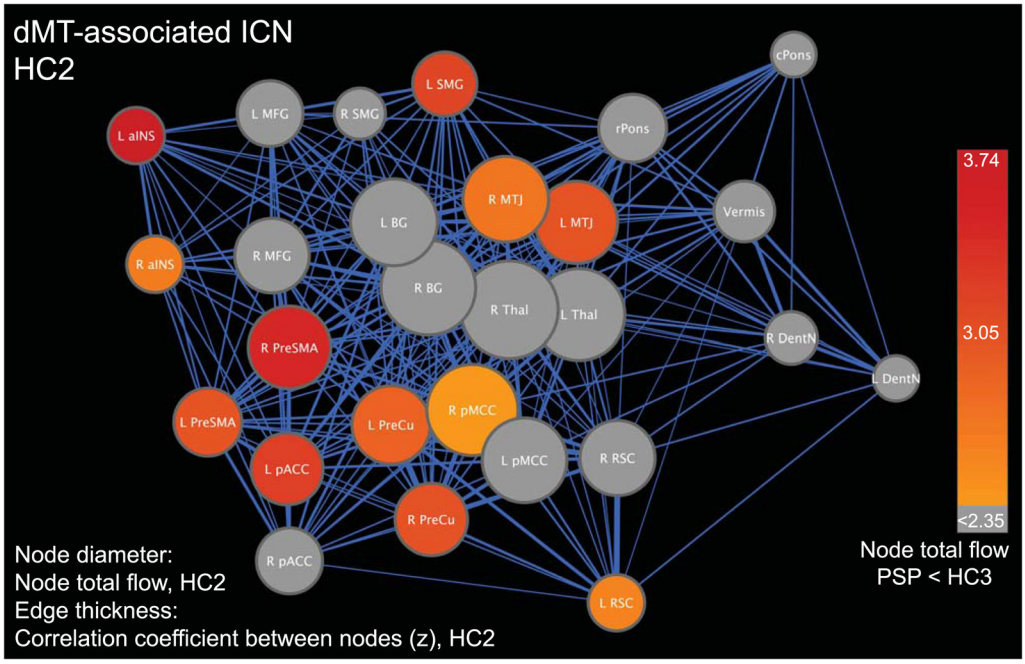

Figure 4. The matrix-derived dMT-associated ICN architecture and connectivity reductions in PSP

An edge-weighted force-directed algorithm was used to display the relationships among network nodes in the healthy brain (HC2 data). Heuristically, nodes clustered together represent more closely related subnetworks and nodes placed centrally within the overall graph have stronger, more numerous edges characteristic of central hubs. Node diameter represents node total flow, whereas edge thickness represents the correlation coefficient of the node pair connected by that edge transformed to z-scores. To overlay PSP-related deficits on the healthy brain graph, nodes were colored by the t-score resulting from the two-sample t-test for node total flow (PSP < HC3) and thresholded at a $p < 0.05$, corrected for false discovery rate across the network. Abbreviations as in Figures 1–3.

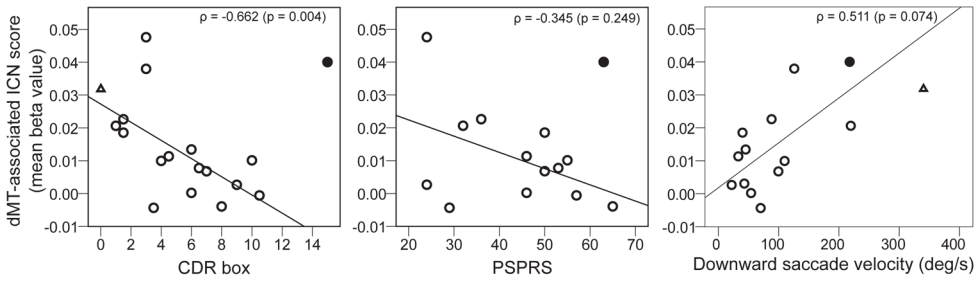

Figure 5. Clinical Correlations to dMT-associated ICN Score

Scatterplots represent the relationships between mean network connectivity and CDR sum of boxes score, PSPRS, and downward saccade velocity. The dMT-associated ICN score was calculated as each subject's mean beta value across all voxels within their dMT-associated ICN map, masked by the ICN as defined in HC2 subjects (see Methods). Circles represent PSP subjects; the one filled circle indicates an outlier excluded from the CDR and PSPRS correlation analyses but included in the downward saccade velocity correlation analysis, in which she was not an outlier. For comparison, the empty triangle represents the mean dMT-associated ICN score for matched control subjects (HC3).

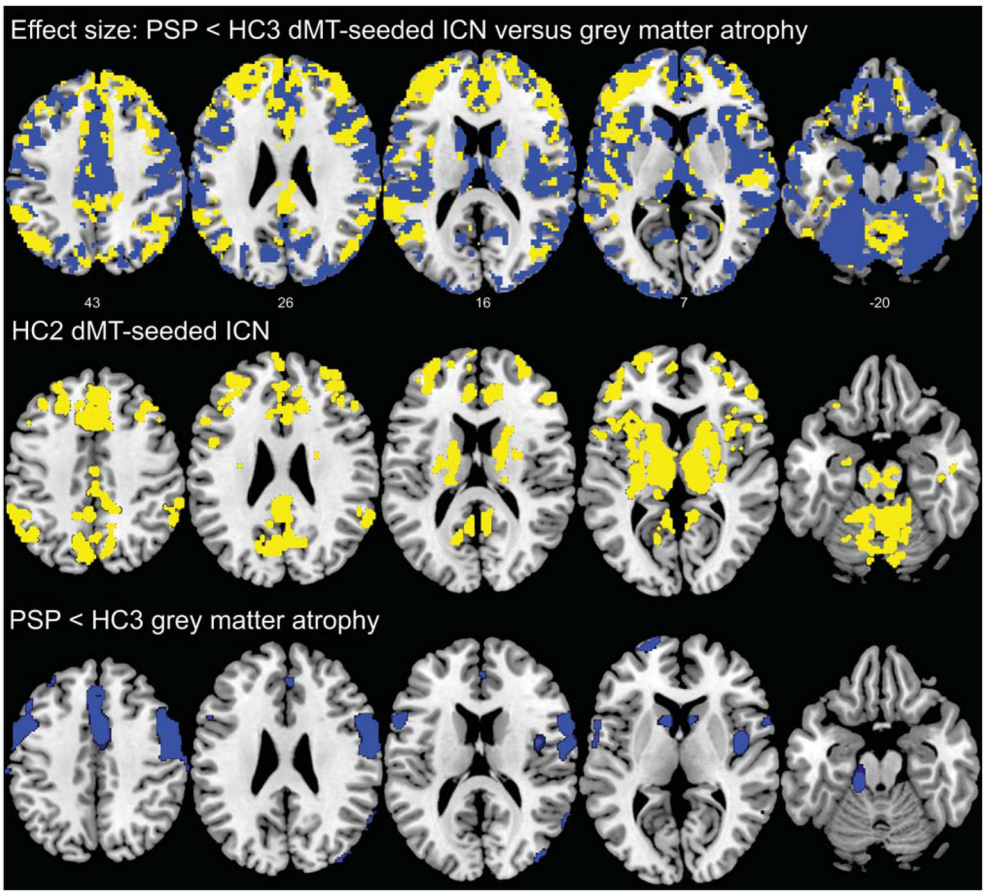

Figure 6. Effect size comparison of dMT associated ICN reductions versus grey matter atrophy in patients with PSP-S compared to matched controls

Upper row: We compared voxel-wise PSP-S < HC3 effect sizes produced by the dMT-associated ICN and VBM grey matter analyses. Voxels where the dMT ICN reduction produced a greater effect size are shown in yellow, whereas voxels where VBM afforded a greater effect size are shown in blue. Effect size maps were thresholded to include only those voxels that had a moderate effect size (0.5) or greater. Middle row: For comparison, we display the corresponding views of the dMT ICN map from the HC2 network discovery group (as shown in Figure 2; height threshold $p < 0.0001$, extent threshold $p < 0.001$, family-wise error-corrected at the cluster level). Bottom row: The corresponding VBM grey matter atrophy pattern in PSP-S compared to HC3 ($p < 0.05$, family-wise error corrected at the voxel level across the whole brain) illustrates the relative structural integrity of regions where ICN methods produced greater effect sizes than VBM. Slice labels reflect MNI coordinates. The right side of the images corresponds to the right side of the brain. Note that the effect size and VBM analyses were conducted on grey matter maps, which exclude most brainstem regions.

Table 1

Table Demographics and neuropsychological features for PSP and matched healthy controls (HC3).

	Healthy controls (HC3) (n=36)	PSP (n=18)	P value, df
Age, years	68.8 (5.7)	67.3 (6.0)	0.394, 52
M:F, n	12:24	6:12	NA
Education, years	16.4 (1.7)	15.8 (2.6)	0.312, 54
Illness duration, years	NA	4.8 (2.3)	NA
PSP-RS	NA	45.0 (13.8)	NA
UPDRS	NA	37.5 (15.1)	NA
Downward saccade velocity, deg/s	340.3 (85.5)	90.0 (65.3)	<0.001, 35
CDR, total	0 (0)	0.94 (0.6)	NA
CDR, sum of boxes	0.01 (0.08)	5.9 (3.7)	NA
MMSE (max = 30)	29.5 (0.8)	26.1 (4.5)	<0.001, 54
CVLT-SF, four learning trials, total (max = 36)	NC	18.5 (11.7)	NA
CVLT-SF, 10 minute recall, score (max = 9)	NC	4.2 (3.0)	NA
Modified Rey-O copy (max = 17)	15.3 (0.9)	11.4 (4.2)	<0.001, 34
Modified Rey-O 10 minute recall (max = 17)	12.6 (2.6)	8.4 (3.7)	0.001, 27
Digit span backward	5.5 (1.4)	3.6 (0.9)	<0.001, 39.4
Modified trails (correct lines per minute)	36.9 (11.6)	13.8 (6.4)	<0.001, 47
Design fluency (max = 30)	10.9 (3.7)	5.8 (2.3)	<0.001, 45
Letter fluency (‘D’ words in 1 minute)	15.5 (5.0)	6.6 (4.8)	<0.001, 40
Semantic fluency (animals in 1 minute)	23.6 (5.3)	10.0 (4.8)	<0.001, 48
Abbreviated BNT (max = 15)	14.7 (0.6)	13.6 (2.2)	0.015, 50
Calculations (max = 5)	4.9 (0.3)	3.9 (0.8)	<0.001, 47
Translational motion (mRMS), mm	0.328 (0.188)	0.328 (0.276)	0.52, 54
Rotational motion (mEuler), degrees	0.13 (0.09)	0.16 (0.15)	0.96, 54

Values represent mean (s.d.). Non-parametric tests used where appropriate.

Abbreviations: BNT, Boston Naming Test; CDR, Clinical Dementia Rating; CVLT-SF, California Verbal Learning Test-Short form; deg/s, degrees per second; mEuler, mean Euler angle; MMSE, Mini-Mental State Examination; mRMS, mean root mean square; NA, not applicable; NC, not collected; PSP-RS, PSP Rating Scale; UPDRS, Unified Parkinson’s Disease Rating Scale.